PHYSICAL REVIEW B **83**, 121408(R) (2011)

Illuminating the dark corridor in graphene: Polarization dependence of angle-resolved photoemission spectroscopy on graphene

Isabella Gierz,[1,*] Jürgen Henk,[2] Hartmut Höchst,[3] Christian R. Ast,[1] and Klaus Kern[1,4]

[1]*Max-Planck-Institut für Festkörperforschung, DE-70569 Stuttgart, Germany*

[2]*Max-Planck-Institut für Mikrostrukturphysik, DE-06120 Halle (Saale), Germany*

[3]*Synchrotron Radiation Center, University of Wisconsin-Madison, Stoughton, Wisconsin 53589, USA*

[4]*IPMC, Ecole Polytechnique Fédérale de Lausanne, CH-1015 Lausanne, Switzerland*

(Received 27 January 2011; published 22 March 2011)

We have used *s*- and *p*-polarized synchrotron radiation to image the electronic structure of epitaxial graphene near the $\overline{K}$ point by angle-resolved photoemission spectroscopy (ARPES). Part of the experimental Fermi surface is suppressed due to the interference of photoelectrons emitted from the two equivalent carbon atoms per unit cell of graphene's honeycomb lattice. Here we show that, by rotating the polarization vector, we are able to illuminate this dark corridor giving access to the complete experimental Fermi surface. Our measurements are supported by first-principles photoemission calculations, which reveal that the observed effect persists in the low-photon-energy regime.

DOI: 10.1103/PhysRevB.83.121408 PACS number(s): 73.22.Pr, 71.15.Mb, 73.20.At, 79.60.−i

Graphene, a single layer of sp^2-bonded carbon atoms, is one of the paradigm two-dimensional (2D) electron systems existing today. It is renowned for its high crystalline quality, its extremely high carrier mobility[1,2] as well as its peculiar charge carriers that behave like massless Dirac particles.[3–7] Graphene's honeycomb lattice consists of two equivalent triangular sublattices, which lead to the description of the charge carriers in terms of spinor wave functions, where the spin index indicates the sublattice rather than the real electron spin, hence the term pseudospin.[8] This pseudospin is responsible for graphene's many intriguing electronic properties. First of all, the difference in pseudospin of the two cosine-shaped bands originating from the two sublattices allows them to cross at the $\overline{K}$ point of the 2D Brillouin zone (see inset of Fig. 1) where they form the conical band structure.[3,4] Second, due to the pseudospin, the charge carriers accumulate a Berry phase of π on closed-loop paths resulting in the absence of backscattering.[9–11] Furthermore, the pseudospin is responsible for the peculiar half-integer quantum Hall effect observed in graphene[5,12] and allows for the observation of Klein tunneling.[13] The pseudospin concept has spawned ideas for different pseudospintronic device proposals such as, e.g., the pseudospin valve.[14]

The effect of the pseudospin is also observed in angle-resolved photoemission spectroscopy (ARPES) experiments. Here, it is rather unwanted because it suppresses the photoemission intensity on part of the Fermi surface (dark corridor[15–17]). The effect was verified many times in ARPES experiments using *p*-polarized light,[6,18–21] and the presence of this dark corridor was never questioned. Unfortunately, the dark corridor effectively prevents the experimental verification of the spin rotation upon quasiparticle to photoelectron conversion in graphene because of the lack of photoemission intensity in the region of interest.[15]

Here we show that, by using *s*-polarized light, it is possible to illuminate this dark corridor and thereby access the complete Fermi surface of graphene in an ARPES experiment. While the dark corridor has been addressed theoretically before,[16,17] the polarization dependence of the intensity modulation on the Fermi surface cannot be accounted for by the single free-electron final state used in this model. We show that this problem is overcome in our first-principles photoemission calculations where we use time-reversed spin-polarized low-energy electron diffraction (SPLEED) states as final states.

A sketch of the experimental setup is displayed in Fig. 1. The measurements were done at the Synchrotron Radiation Center (SRC) in Stoughton, Wisconsin, at the variable polarization VLS-PGM beamline. This beamline is equipped with an elliptically polarized Apple II undulator that delivers *p* and *s* polarization of photons in an energy range from 15 to 250 eV. For *s*- (*p*-) polarized light, the electric field vector lies perpendicular to the plane of incidence (in the plane of incidence) spanned by the sample normal and the direction of incidence of the light. To measure the photoemission current as a function of k_y, the sample was rotated by an angle θ (see Fig. 1). The k_x direction (perpendicular to the paper plane in Fig. 1) corresponds to the angular dispersion direction on the 2D detector. The angular resolution of 0.4° translates into a wave-vector resolution at the Fermi level of 0.016 Å^{-1} for $h\nu = 35$ eV and of 0.022 Å^{-1} at $h\nu = 52$ eV. The energy resolution of the complete setup is better than 10 meV. During measurements, the sample was kept at a temperature of 50 K. We have grown graphene by thermal decomposition of SiC(0001) in ultrahigh vacuum.[22,23] Details of the sample preparation are reported in Refs. 20 and 24.

First-principles electronic-structure calculations have been performed for a free-standing graphene layer within the framework of relativistic multiple-scattering theory (layer Korringa-Kohn-Rostoker method[25,26]) using the Perdew-Wang exchange-correlation potential.[27] The self-consistent potentials serve as input for the photoemission calculations, which rely on the relativistic one-step model.[25,28] Thus, all essential ingredients of the excitation process are captured in particular transition matrix elements and boundary conditions. Many-body effects are incorporated via the complex self-energy Σ. The imaginary part of Σ is taken as 1.5 eV for the final state (time-reversed SPLEED state) and as 0.01 eV for the initial state (graphene orbitals); its real part is assumed

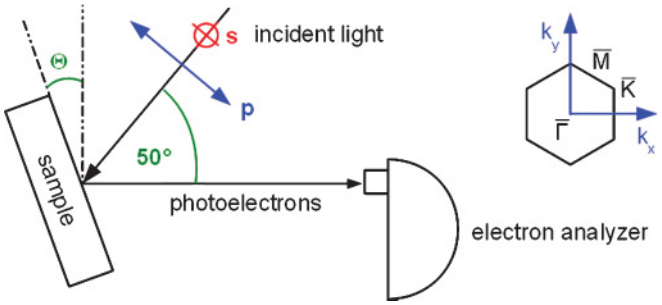

FIG. 1. (Color online) Sketch of the experimental setup. For s- (p-) polarized light, the electric field vector lies perpendicular to the plane of incidence (in the plane of incidence) spanned by the sample normal and the direction of incidence of the light. The inset shows the 2D Brillouin zone.

zero. Including a nonzero real part of the self-energy would shift the final states to higher energies. Furthermore, the final state in experiment is scattered by the SiC substrate, so that deviations between the theoretical and experimental final states are possible. These deviations may include slight changes in the final-state composition as well as the band dispersion. Nevertheless, trends in experiment are fully accounted for, in particular, the photon energy dependence of the intensities. For a direct comparison between experiment and theory, the theoretical photon energies $h\nu_{\text{th}}$ have been shifted by 8.6 eV toward higher photon energies.

Figure 2 shows the measured band structure for an epitaxial graphene monolayer on SiC(0001) along the $\overline{\Gamma K M}$-direction. As epitaxial graphene on SiC(0001) is slightly n-doped due to charge transfer from the substrate, the crossing point of the

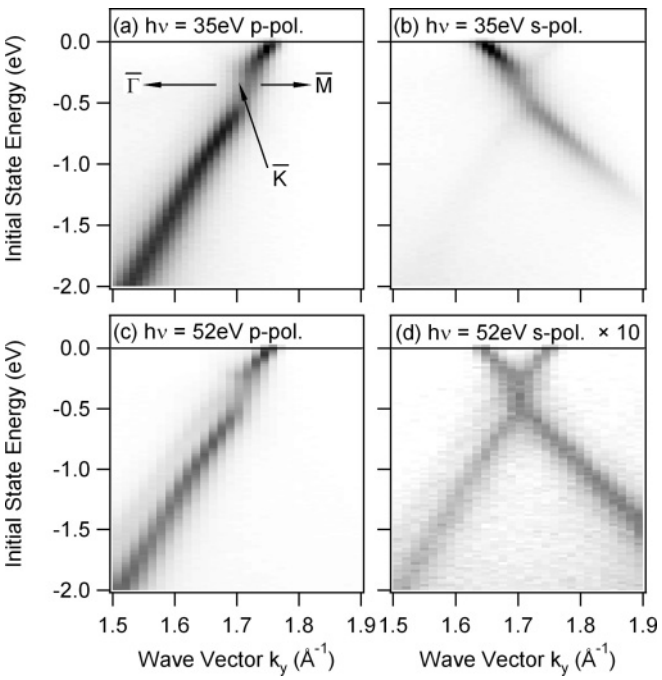

FIG. 2. Band structure measured along $\overline{\Gamma K}$ for an epitaxial graphene monolayer on SiC(0001) for two different photon energies [(a), (b): 35 eV; (c), (d): 52 eV] for both p-polarized [(a), (c)] and s-polarized [(b), (d)] light. The gray scale is linear with black (white) corresponding to high (low) photoemission intensities.

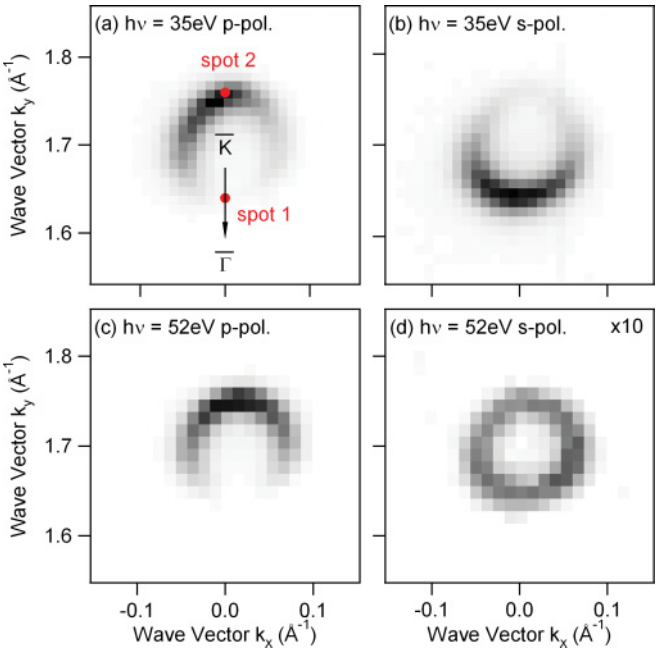

FIG. 3. (Color online) Fermi surface of epitaxial graphene on SiC(0001) measured with p-polarized light [(a), (c)] and s-polarized light [(b), (d)] for two different photon energies [(a), (b): 35 eV; (c), (d): 52 eV]. The gray scale is linear with black (white) corresponding to high (low) photoemission intensities.

two linearly dispersing π bands is located at about -420 meV below the Fermi level.[6,18,20,21] The data in Fig. 2 were recorded at a photon energy of $h\nu = 35$ eV with p- and s-polarized light. The gray scale is linear with black (white) corresponding to high (low) photoemission intensities. For p-polarized photons [Figs. 2(a) and 2(c)], the intensity for one of the two branches is completely suppressed due to interference effects in the photoemission process,[16,17] and only the branch dispersing upward (towards the Fermi level) along $\overline{\Gamma K M}$ is visible in agreement with previous photoemission results.[6,18–21] For $h\nu = 35$ eV and s-polarized light [Fig. 2(b)], the photoemission intensity shifts to the second branch dispersing downward (away from from the Fermi level) along $\overline{\Gamma K M}$ that was invisible when using p-polarized light. When using s-polarized light at $h\nu = 52$ eV [Fig. 2(d)], both π bands are visible. In this case, the overall intensity is reduced by about one order of magnitude as compared to the other measurements.

Figure 3 shows the corresponding Fermi surfaces around $\overline{K}$ for $h\nu = 35$ and 52 eV with both p- and s-polarized light. For p-polarized radiation [Figs. 3(a) and 3(c)], there is no photoemission intensity at spot 1. This situation changes drastically when using s-polarized photons with $h\nu = 35$ eV in Fig. 3(b). In this case, there is no photoemission intensity at the opposite side of the Fermi surface at spot 2. Changing the photon energy to $h\nu = 52$ eV leads to a homogeneous illumination of the complete Fermi surface with s-polarized light [Fig. 3(d)]. As in Fig. 2(d), the photocurrent is one order of magnitude lower than for p-polarized radiation. As can be seen, the dark corridor at spot 1 (as introduced by Refs. 15–17) can be illuminated using s-polarized light.

The origin of the dark corridor has been explained by calculating the photoemission matrix element in dipole

approximation using atomic orbitals for the initial state and a single plane wave for the final state.[16] It has been shown that the photoemission intensity around $\overline{K}$ can be separated into a polarization factor and an interference term related to the crystal structure. The interference term is responsible for the suppression of the photocurrent at spot 1 at the Fermi energy. The polarization factor $(\boldsymbol{k}\hat{\lambda})$ implies that the photoemission intensity vanishes completely for $\boldsymbol{k} \perp \hat{\lambda}$, i.e., for s-polarized radiation. While this model explains the results for p-polarized light very nicely, our results show that this simple picture does not hold for s-polarized light.

For better agreement with the experimental findings, we have used time-reversed SPLEED states as final states. Figure 4 shows the calculated Fermi surface for p- and s-polarized light with $h\nu = 35$ and 52 eV. The calculation is in good agreement with the experimental results in Fig. 3. The dark corridor lies at spot 1 (spot 2) for p-polarized (s-polarized $h\nu = 35$ eV) light. For s-polarized light at $h\nu = 52$ eV, the Fermi surface is completely illuminated. To complete the picture, Fig. 4(e) shows the intensity asymmetry between spots 1 and 2 defined as $A = (I_{\text{spot1}} - I_{\text{spot2}})/(I_{\text{spot1}} + I_{\text{spot2}})$ as a function of photon energy. For $A = \pm 1$, the dark corridor lies at spot 1 or spot 2, respectively. For $A = 0$, spots 1 and 2 are equally illuminated, which is the case for $h\nu = 52$ eV and s-polarized light. The effect that spot 1 can be illuminated using s-polarized light persists for photon energies between $h\nu = 24$ and 52 eV. The narrow peaks at 24 and 57 eV in Figs. 4(e) and 4(g) originate from beam emergence thresholds in the final state.[29] The disappearance of the effect for $h\nu > 52$ eV is attributed to a change in the final states. Decomposing the time-reversed SPLEED final states into angular-momentum partial waves, we find that, for $h\nu < 52$ eV, s-like partial waves dominate the photoemission process, while, for $h\nu > 52$ eV, the contributions from d-like partial waves dominate [see Fig. 4(f)].

To compare our calculations with the results from Ref. 16, we project the time-reversed SPLEED final states onto free-electron final states. This decomposition shows that the photoemission process is dominated by up to 12 different plane waves, the relative weight of which depends on the photon energy, in contrast to the single plane wave used in Ref. 16. In agreement with the previous partial-wave decomposition and earlier results from Ref. 30, we find a transition between different plane-wave contributions around $h\nu = 52$ eV. The single plane wave used in Ref. 16 contributes at all photon energies, which explains the success of the model for p-polarized light. However, in order to explain the experimental results for s-polarized light within a tight-binding calculation, it is necessary to employ more than just one plane-wave final state. Detailed calculations are given as in Ref. 31.

Figure 4(g) shows the relative intensity of spot 1 compared to spot 2 as a function of photon energy. The photoemission intensity at spot 1 does not go to zero but remains at a few percent for p-polarized light and photon energies below

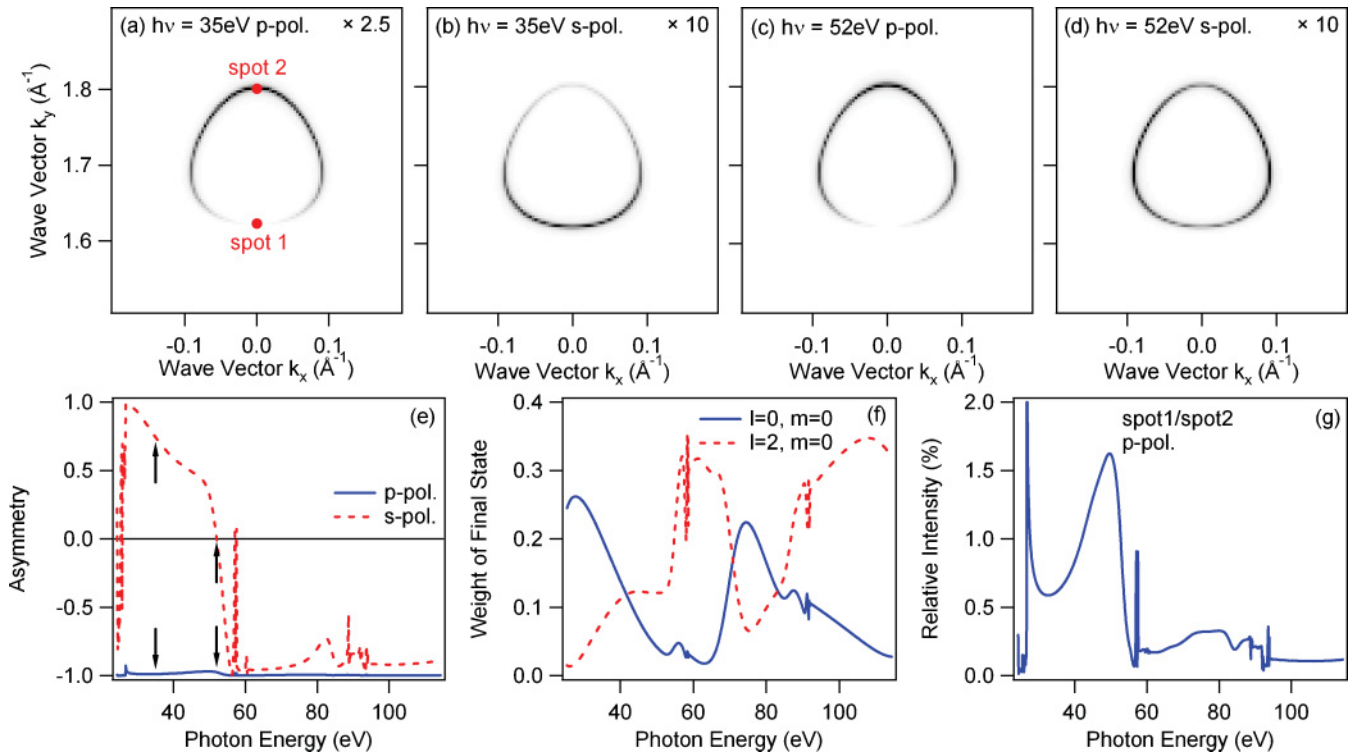

FIG. 4. (Color online) Photoemission calculations of the Fermi surfaces for p-polarized [(a), (c)] and s-polarized [(b), (d)] radiation for $h\nu = 35$ eV [(a), (b)] and $h\nu = 52$ eV [(c), (d)]. Panels (e), (f), and (g) show the intensity asymmetry of spots 1 and 2 (blue/continuous lines: p-polarized light; red/dashed lines: s-polarized light), the relevant final-state contributions for linearly polarized light (blue/continuous lines: $l = m = 0$; red/dashed lines: $1 = 2$, $m = 0$), as well as the intensity ratio of spot 1 compared to spot 2 for p-polarized light, respectively, as a function of photon energy. The theoretical photon energies have been shifted by 8.6 eV to allow for a direct comparison with experiment.

$h\nu = 60$ eV, even though perfect AB sublattice symmetry is assumed. This is in contrast to the tight-binding calculation in Ref. 16, where perfect AB sublattice symmetry leads to zero intensity in the dark corridor. This discrepancy can be understood by including the spin-orbit interaction (SOI) in the tight-binding model.[31] As a result, the wave-function coefficients c_A and c_B of the p_z orbitals centered at the A and B sublattices, respectively, are not equal in magnitude anymore, which leads to a nonzero photocurrent inside the dark corridor. Therefore, ARPES measurements can determine an upper limit for the degree of AB sublattice symmetry breaking.[18,21] A quantitative determination of this symmetry-breaking factor, however, would require a precise knowledge of the SOI. Nevertheless, the assessment of AB symmetry breaking can be improved by going to higher photon energy, where the SOI contribution is less important, as shown in Fig. 4(g).

Furthermore, Ref. 15 predicts a giant spin rotation during quasiparticle to photoelectron conversion in graphene due to spin-pseudospin interference in the photoemission process. Inside the dark corridor (at spot 1), the spin orientation of the photoelectron differs from the spin of the quasiparticle in the initial state by 180°. However, up to now this effect was believed not to be accessible in a spin-resolved ARPES measurement because of the lack of photoemission intensity inside the region of interest. Using s-polarized radiation in a spin-resolved ARPES experiment should allow for the experimental verification of the predicted spin rotation.

In conclusion, we could show that it is possible to illuminate the dark corridor on the measured Fermi surface of graphene using s-polarized synchrotron radiation. This effect is not included in the theoretical model from Ref. 16 that is based on a single free-electron final state. Our first-principles photoemission calculations use time-reversed SPLEED states as final states and result in good agreement with the measured Fermi surfaces. In addition, the calculations reveal that the observed effect persists in the low-photon-energy regime up to about $h\nu = 52$ eV. Furthermore, our findings open up a new pathway to access the giant spin rotation predicted in Ref. 15 experimentally in a spin-resolved ARPES measurement.

The authors thank U. Starke and C. Riedl from the Max Planck Institute for Solid State Research in Stuttgart as well as C. L. Frewin, C. Locke, and S. E. Saddow of the University of South Florida for hydrogen etching of the SiC substrates. C. R. A. acknowledges funding by the Emmy-Noether-Program of the Deutsche Forschungsgemeinschaft (DFG). This work was based in part upon research conducted at the Synchrotron Radiation Center of the University of Wisconsin-Madison, which was funded by the National Science Foundation under Award No. DMR-0537588.

*Corresponding author: i.gierz@fkf.mpg.de

[1] K. S. Novoselov, A. K. Geim, S. V. Morozov, D. Jiang, Y. Zhang, S. V. Dubonos, I. V. Grigorieva, and A. A. Firsov, Science **306**, 666 (2004).

[2] C. Berger *et al.*, Science **312**, 1191 (2006).

[3] P. R. Wallace, Phys. Rev. **71**, 622 (1947).

[4] J. C. Slonczewski and P. R. Weiss, Phys. Rev. **109**, 272 (1958).

[5] K. S. Novoselov, A. K. Geim, S. V. Morozov, D. Jiang, M. I. Katsnelson, I. V. Grigorieva, S. V. Dubonos, and A. A. Firsov, Nature (London) **438**, 197 (2005).

[6] A. Bostwick, T. Ohta, T. Seyller, K. Horn, and E. Rotenberg, Nat. Phys. **3**, 36 (2007).

[7] M. Sprinkle *et al.*, Phys. Rev. Lett. **103**, 226803 (2009).

[8] A. K. Geim and K. S. Novoselov, Nat. Mater. **6**, 183 (2007).

[9] K. Y. Bliokh, Phys. Lett. A **344**, 127 (2005).

[10] S. V. Morozov, K. S. Novoselov, M. I. Katsnelson, F. Schedin, L. A. Ponomarenko, D. Jiang, and A. K. Geim, Phys. Rev. Lett. **97**, 016801 (2006).

[11] I. Brihuega, P. Mallet, C. Bena, S. Bose, C. Michaelis, L. Vitali, F. Varchon, L. Magaud, K. Kern, and J. Y. Veuillen, Phys. Rev. Lett. **101**, 206802 (2008).

[12] X. Wu, Y. Hu, M. Ruan, N. K. Madiomanana, J. Hankinson, M. Sprinkle, C. Berger, and W. A. deHeer, Appl. Phys. Lett. **95**, 223108 (2009).

[13] M. I. Katsnelson, K. S. Novoselov, and A. K. Geim, Nat. Phys. **2**, 620 (2006).

[14] P. San-Jose, E. Prada, E. McCann, and H. Schomerus, Phys. Rev. Lett. **102**, 247204 (2009).

[15] F. Kuemmeth and E. I. Rashba, Phys. Rev. B **80**, 241409(R) (2009).

[16] E. L. Shirley, L. J. Terminello, A. Santoni, and F. J. Himpsel, Phys. Rev. B **51**, 13614 (1995).

[17] H. Daimon, S. Imada, H. Nishimoto, and S. Suga, J. Electron. Spectrosc. Relat. Phenom. **76**, 487 (1995).

[18] T. Seyller, A. Bostwick, K. V. Emtsev, K. Horn, L. Ley, J. L. McChesney, T. Ohta, J. D. Riley, E. Rotenberg, and F. Speck, Phys. Status Solidi B **245**, 1436 (2008).

[19] M. Mucha-Kruczyński, O. Tsyplyatyev, A. Grishin, E. McCann, V. I. Falko, A. Bostwick, and E. Rotenberg, Phys. Rev. B **77**, 195403 (2008).

[20] I. Gierz *et al.*, Phys. Rev. B **81**, 235408 (2010).

[21] A. Bostwick, T. Ohta, J. L. McChesney, K. V. Emtsev, T. Seyller, K. Horn, and E. Rotenberg, New J. Phys. **9**, 385 (2007).

[22] C. Berger *et al.*, J. Phys. Chem. B **108**, 19912 (2004).

[23] K. V. Emtsev, F. Speck, T. Seyller, L. Ley, and J. D. Riley, Phys. Rev. B **77**, 155303 (2008).

[24] I. Gierz, C. Riedl, U. Starke, C. R. Ast, and K. Kern, Nano Lett. **8**, 4603 (2008).

[25] J. Henk, in *Handbook of Thin Film Materials*, edited by H. S. Nalwa (Academic, New York, 2002), Vol. 2, p. 479.

[26] J. Zabloudil, R. Hammerling, L. Szunyogh, and P. Weinberger, *Electron Scattering in Solid Matter* (Springer, New York, 2005).

[27] J. P. Perdew and Y. Wang, Phys. Rev. B **45**, 13244 (1992).

[28] J. Braun, Rep. Prog. Phys. **59**, 1267 (1996).

[29] G. Malmström and J. Rundgren, J. Phys. C: Solid State Phys. **13**, L61 (1980).

[30] N. Barrett, E. E. Krasovskii, J.-M. Themlin, and V. N. Strocov, Phys. Rev. B **71**, 035427 (2005).

[31] See supplemental material at [http://link.aps.org/supplemental/10.1103/PhysRevB.83.121408] for a detailed tight-binding calculation.